ESTIMATING HEAT FLUXES FROM ARIEL'S LARGE CHASMATA. Chloe B. Beddingfield[1,2], Richard J. Cartwright[1], Erin J. Leonard[3], Tom A. Nordheim[3], Francesca Scipioni[1], [1]The SETI Institute, Mountain View, CA (chloe.b.beddingfield@nasa.gov), [2]NASA Ames Research Center, Moffett Field, CA, [3]Jet Propulsion Laboratory, Pasadena, CA.

Introduction: As shown in Voyager 2 Imaging Science System (ISS) images of Ariel's southern hemisphere, the surface is dominated by many sets of large canyons, termed chasmata, bounded by large extensional normal faults (**Fig. 1a**) [e.g., 1-3]. These canyons are up to 3-4 km in depth [4] and hundreds of kilometers in length. Ariel's chasmata exhibit smooth floors, and in some locations, medial grooves that are flanked by parallel ridges, in a double ridge morphology similar to double ridges on Europa and Triton [3].

Ariel's heat flux has been estimated at the location of Korrigan Chasma [5], which is part of the older Pixie Group of canyons. As summarized in [5], the estimated lithospheric thickness and heat flux of Ariel in this location is 3.8-4.4 km and 28-92 mW/m^2, respectively. However, neither current nor hypothesized past tidal heating of Ariel, nor radiogenic heat production are enough to cause these high heat fluxes [5].

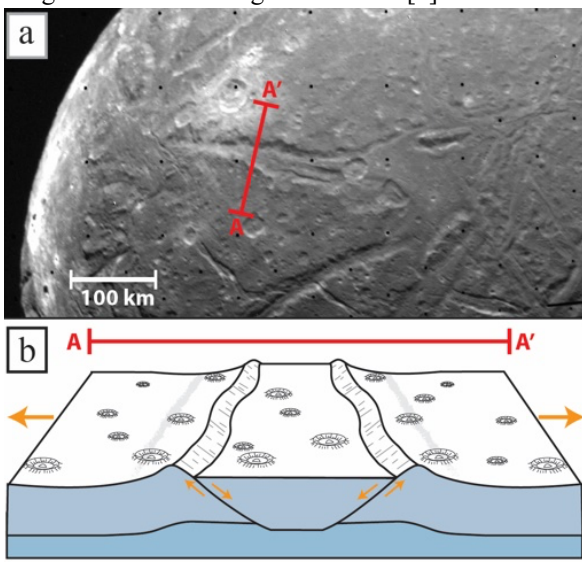

Fig. 1: (a) A Voyager 2 ISS image that covers Sylph Chasma on Ariel. (b) Example of an interpreted cross-sectional structure across profile line A-A' in (a).

Objectives: In this work, we further investigated Ariel's heat fluxes, focusing on locations that exhibit large canyons, including the youngest canyon identified on Ariel, Kachina Chasmata. We identified flexural uplift along the large canyon walls that include Kewpie, Brownie, Kra, Pixi, Sylph, and Kachina Chasmata, and two unnamed chasmata based on four digital elevation models (DEMs) developed for this work (**Fig. 2**). We conducted morphometric measurements of these canyons to estimate heat fluxes in different regions, which may have different lithospheric properties, shaped during different periods of Ariel's geologic history.

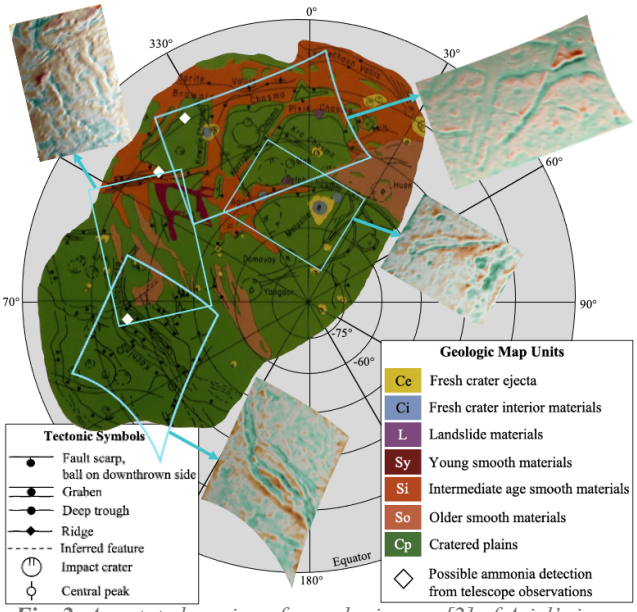

Fig. 2: Annotated version of a geologic map [2] of Ariel's imaged southern hemisphere. The locations of the DEMs (cyan boxes) generated for this work are shown. The locations of possible ammonia detections are summarized in [10].

Methods: We used similar techniques to those developed for estimating heat fluxes using flexural modeling [5-7]. This method is applicable to features that display lithospheric flexure (**Fig. 1b**). Therefore, we applied the methodology described by [8] to use flexural curvature to estimate the thicknesses of the elastic and mechanical layers. These thickness estimates were used to estimate lithospheric heat flux.

The bending moment of the elastic layer is given by

$$M = \frac{E K_{max}\, T_e^3}{12\,(1-\nu^2)}$$

where E is the Young's modulus, which is similar for NH_3-hydrates and pure H_2O at cryogenic temperatures [9], K_{max} is the maximum curvature of the topography, T_e is the effective elastic thickness, and ν is Poisson's ratio. The bending moment of the elastic layer is equivalent to the bending moment of the mechanical lithosphere, which is given by

$$M = \int_0^{T_m} \sigma(z)\,(z - z_n)\,dz$$

where T_m is the mechanical thickness of the lithosphere, $\sigma(z)$ is fiber stress, which is the differential stress at

depth z, and σ(z) is the depth to the neutral stress plane, where σ(z) = 0. The fiber stress is given by

$$\sigma_{(z)} = \frac{E\,K\,(z - z_n)}{1 - \nu^2}$$

and is imposed at the condition of zero net axial force, where $\int_0^{T_m} \sigma(z)\,dz = 0$. The elastic layer bending moment is equivalent to that of the mechanical layer, therefore the effective elastic thickness is given by

$$T_e = \left\{ \frac{12\,(1-\nu^2)}{E\,K_{max}} \int_0^{T_m} \sigma(z)\,(z - z_n)\,d_z \right\}^{1/3}$$

where T_m is the mechanical thickness. The temperature at the base of the lithosphere is given by

$$T_b = \frac{Q_a}{n\,R}\left[\ln\left(\frac{3\,D_e\,\mu\,A^{\frac{1}{n}}}{\dot{\varepsilon}^{\frac{1}{n}}\,d^{\frac{P}{n}}}\right)\right]^{-1}.$$

From these equations, the thermal gradient can by calculated where $\Delta T = \frac{T_b - T_s}{d}$, and the heat flux where $F = k_c \frac{(T_b - T_s)}{T_e}$. We chose the k_c values for NH_3-hydrates and pure H_2O ice based on results of our analysis of reflectance spectra of Ariel [10].

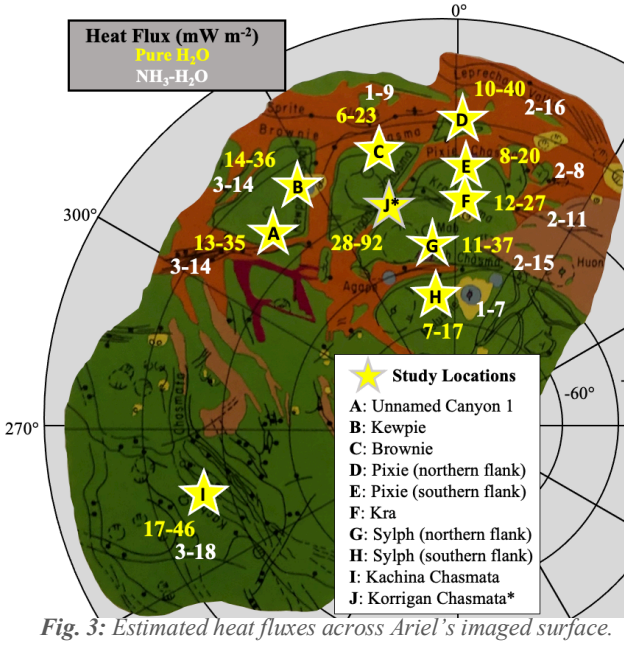

Fig. 3: *Estimated heat fluxes across Ariel's imaged surface.*

Results: We estimate that Ariel's elastic thickness ranges from 4.4±0.3 km to 11.4±1.4 km across the imaged region (**Fig. 3**). The Kachina Group, the younger set of faults, has a relatively low elastic thickness of 4.4±0.7 km when compared to many chasmata in the older Pixie Group. In the Pixie Group, elastic thickness values range from 4.1±0.3 km to 11.4±1.4 km. The regions where the lithosphere has the highest elastic thickness values include the vicinity of Brownie Chasma (10.3±3.0 km), south of Pixie Chasma (9.7±1.3 km), and south of Sylph Chasma (11.4±1.4 km). The central region exhibits evidence for a thinner elastic layer, including the region around the Unnamed Canyon (5.7±1.0 km), Kewpie Chasma (5.3±0.6 km), and Korrigan Chasma (4.1±0.3, estimated by [5]).

Our results indicate that a pure water ice lithosphere would correspond to heat fluxes ranging from 17-46 mW m^{-2} for the Kachina Group and 6-40 mW m^{-2} for the Pixie Group. Work by [5] estimated heat fluxes for Korrigan Chasma, also in the Pixie group, ranging from 28-92 mW m^{-2}. Alternatively, if some ammonia-bearing species are present in Ariel's lithosphere, then the estimated heat fluxes are lower, ranging from 3-18 mW m^{-2} for the Kachina Group and 1-16 mW m^{-2} for the Pixie Group.

Future Work: We will extend our work to estimating heat fluxes on Ariel's neighboring satellite, Miranda. We have identified evidence for flexure on the large canyon that bounds Inverness Corona (**Fig. 4**), which is thought to be the youngest corona on Miranda imaged by Voyager 2. We will estimate the elastic thickness, thermal gradient, and heat flux of this region using flexural modeling. We will then compare these results to newly mapped features in this region (see abstract by Leonard et al. for LPSC 2022) to better constrain the geologic history of Inverness Corona.

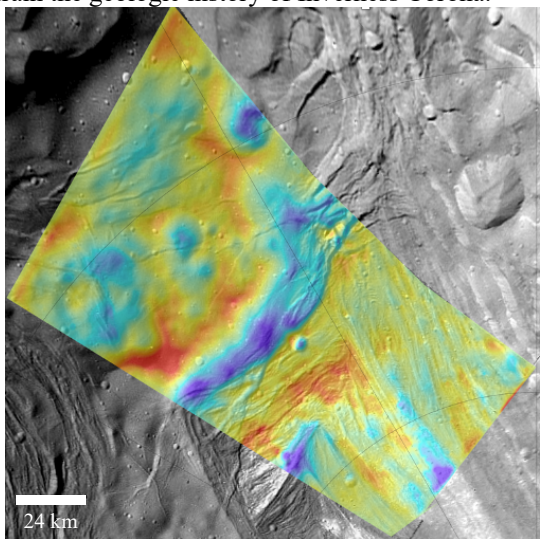

Fig. 4: *DEM of Miranda's Inverness Corona. The relative elevation ranges from 0 km (purple) to 4 km (red).*

Acknowledgements: NASA Solar System Workings (SSW) grant NHH18ZDA001N for the work on Ariel and JPL Strategic Research & Technology Development Program grant SI-2021-028-yr2 for Miranda.

References: [1] Smith et al. (1986) *Science*, 233, 43-64. [2] Croft & Soderblom (1991) *Uranus*, 561-628. [3] Beddingfield & Cartwright (2021) *Icarus*, 367, 114583. [4] Thomas (1988) *Icarus*, 73, 427-441. [5] Peterson et al. (2015) *Icarus*, 250, 116-122. [6] Ruiz (2005) *Icarus*, 177, 438-446. [7] Giese et al. (2007) *GRL*, 34, L21203. [8] McNutt (1984) *JGR*, 89, 11180-11194. [9] Lorenz & Shandera (2001) *GRL*, 28, 215-218. [10] Cartwright et al. (2020) *ApJL*, 898, l22.